

Interpreting the 95 GeV resonance in the Two Higgs Doublet Model

Implications for the Electroweak Phase Transition

Ansh Bhatnagar[Ⓧ],^{a,*} Djuna Croon[Ⓧ],^{a,†} and Philipp Schicho[Ⓧ]^{b,‡}

^a*Institute for Particle Physics Phenomenology, Department of Physics,
Durham University, Durham DH1 3LE, U.K.*

^b*Département de Physique Théorique, Université de Genève,
24 quai Ernest Ansermet, CH-1211 Genève 4, Switzerland*

Abstract

We investigate if the recent mass resonance excesses seen around 95 GeV at the Large Hadron Collider (LHC) can be reconciled with a first-order electroweak phase transition. Performing the first large-scale parameter scan of the Two Higgs Doublet Model (2HDM) using high-temperature dimensionally reduced effective field theory, we focus on regions of parameter space consistent with interpreting the excess as an additional pseudoscalar state. We find that, in contrast to the Standard Model, the electroweak transition pattern in the 2HDM is generically first-order, proceeding either in a single or in two steps. While transition strengths can reach up to $v_c/T_c \sim 1.3$, the gravitational wave signals lie below the projected reach of future interferometer experiments and are likely insufficient to support successful electroweak baryogenesis.

*ansh.bhatnagar@durham.ac.uk

†djuna.l.croon@durham.ac.uk

‡philipp.schicho@unige.ch

Contents

1	Introduction	2
2	Two Higgs Doublet Model	3
3	The 2HDM thermal potential	6
3.1	The dimensionally reduced effective potential	7
3.2	Higher-orders in the effective potential	8
4	Bubble Nucleation and Gravitational Waves	9
4.1	Bubble nucleation	9
4.2	Gravitational Wave spectrum	12
4.3	From dimensionally reduced potential to gravitational waves	13
5	Parameter scans	14
6	Conclusions	19
A	Renormalisation of the 2HDM	21
A.1	Running and β -functions	21
A.2	Relations between $\overline{\text{MS}}$ -parameters and physical observables	22
B	Integration of DR EFT into PhaseTracer2	23

1. Introduction

Following the discovery of the Higgs boson [1, 2], searches at the Large Hadron Collider (LHC) have increasingly focused on exploring the structure of the Higgs sector. Motivated by numerous Beyond the Standard Model (BSM) scenarios featuring extended scalar sectors, the CMS collaboration extended its Higgs-like particle searches to include invariant masses below 110 GeV. While CMS reported an excess near 95 GeV in the diphoton channel by combining data from 8 and 13 TeV runs with a local significance of 2.8σ [3], recently, this result was updated using the full 13 TeV dataset. The latter shifted the excess to 95.4 GeV with a local significance of 2.9σ [4]. The presence of a neutral scalar decaying into two photons around 95 GeV remains compatible with the latest ATLAS results [5].

A resonance of a similar mass has also been reported by CMS in $\tau\tau$ final state searches at around 100 GeV [6], and around 98 GeV in $b\bar{b}$ final state searches at the Large Electron-Positron (LEP) collider in 2006 [7].

Due to the limited resolution of the CMS and LEP measurements, these measurements seem to be compatible and could point to a new scalar particle at a mass of around 95 GeV. The possibility of a lighter Higgs-like particle explaining these excesses has been explored in numerous models [8–29].

A model that has been studied extensively in the context of new Higgs-like particles is the Two Higgs Doublet Model (2HDM), a minimal extension to the Standard Model that requires the addition of an extra Higgs doublet [10, 11, 13, 23, 25–29]. This model predicts additional scalar particles, which may account for a 95 GeV resonance. Although phenomenological investigations of the 2HDM in this context have largely focused on collider observables [10, 29], the existence of new scalars coupled to the Higgs can also alter the dynamics of cosmological evolution.

In this work, we explore the possibility of a first-order electroweak phase transition (EWPT) in the Type I 2HDM model, identifying the 95 GeV excess with an additional pseudoscalar state. Employing state-of-the-art dimensional reduction to a three-dimensional effective field theory (3D EFT) [30, 31], we perform a broad finite-temperature scan over the parameter region compatible with current collider limits.

Previous studies have explored the EWPT in the 2HDM using both perturbative and non-perturbative approaches. Early work using one-loop finite-temperature effective potentials (e.g. [32–38]) showed that a strong first-order EWPT is possible in Type-I and Type-II 2HDMs, typically requiring sizable mass splittings among the scalar states to enhance thermal barriers generated by gauge bosons or scalar loops (e.g. [32, 36]). These studies often focused on parameter regions with heavy new scalars with $M \gtrsim 300$ GeV, motivated by electroweak precision tests [39–43] and Higgs signal strength measurements.

More recently, non-perturbative studies of the dimensionally reduced 3D EFT have been

employed to assess the nature of the electroweak phase transition more reliably; see e.g. [44–47] for recent analyses, or [48–50] for earlier foundational work. The model has also been studied perturbatively, including in its inert doublet realisation [51–53].

These studies have demonstrated that certain regions of 2HDM parameter space can indeed support a strong first-order electroweak phase transition, particularly when thermally induced cubic terms in the potential are sufficiently enhanced. However, such analyses typically do not account for the presence of a light scalar or pseudoscalar near 95 GeV, nor the associated phenomenological constraints.

The potential existence of such a light state can substantially alter the structure of the finite-temperature potential. In particular, it can introduce new phase transition pathways or weaken the strength of the transition by reducing the need for large mass splittings.

We find that unlike in the Standard Model, where the EWPT is a crossover [54–58], the transition is first order in the majority of the parameter space. Moreover, depending on the parameters in the 2HDM Lagrangian, the transition can occur in a single or in two steps; see [59] for a non-perturbative analysis of two-step transitions in the triplet extension of the SM. We find that the transition strength remains modest across the viable parameter space, with the order parameter not exceeding $v_c/T_c \lesssim 1.3$.

A strong first-order phase transition can leave behind a stochastic gravitational wave (GW) background. However, due to the relatively modest values of the order parameter in the 2HDM, the resulting GW signal lies well below the projected sensitivity of LISA [60–62] and other planned (space-based) observatories [63–65]; see [66–70] for recent discussions of GW prospects in the 2HDM context.

Furthermore, the moderate strength of the transition also appears insufficient to support another potential remnant of a strong first-order transition, electroweak baryogenesis. Achieving successful baryogenesis would likely require additional model ingredients, such as tree-level barriers in the effective potential, to sufficiently enhance the strength of the transition and realise a sharp turn-off of the electroweak sphaleron rates inside the bubbles of true vacuum. We discuss possible extensions, including singlet scalars or higher-dimensional operators, that could enhance the transition.

2. Two Higgs Doublet Model

The real Two Higgs Doublet Model (2HDM) Type I is particularly well suited to accommodating a new ~ 95 GeV state while respecting existing flavour and collider bounds. In Type I, all fermions couple to the same Higgs doublet, so the stringent $b \rightarrow s\gamma$ constraints that force charged Higgses above a few hundred GeV in Type II/Flipped models are much weaker here – allowing $m_{H^\pm} \sim 150 - 350$ GeV alongside a light neutral scalar or pseudoscalar. Moreover, imposing the alignment limit $|\cos(\beta - \alpha)| \ll 1$ keeps the 125 GeV Higgs SM-like,

while still permitting a new state at 95 GeV with suppressed couplings to VV and enhanced loop-induced couplings to $\gamma\gamma$ and $\tau\tau$.

In this work, we explore the scenario in which the pseudoscalar A is identified with the new 95 GeV resonance. This assignment provides a better fit to existing collider data compared to associating the scalar H with the resonance. The reason is as follows. In the $m_H = 95$ GeV scenario, the CP-even scalar H couples to electroweak vector bosons at tree level. However, these couplings are constrained by the Higgs signal-strength sum rule and by global fits to Higgs data (see e.g. [25]) which restrict the scalar mixing via $|\cos(\beta - \alpha)| \lesssim 0.2$. This suppression limits both the production cross section and the branching ratio into $\gamma\gamma$, making it difficult to account for either the LEP excess in the $b\bar{b}$ channel [7] or the diphoton excess observed by CMS [25].

The Higgs sector of the 2HDM consists of two $SU(2)_L$ doublets, Φ_1 and Φ_2 , with opposite charge under a \mathbb{Z}_2 symmetry and hypercharge $Y = 1/2$. All right-handed SM fermions are taken to be even under the \mathbb{Z}_2 , while Φ_1 is conventionally chosen to be odd, making it a fermiophobic doublet. Thus the resulting Yukawa terms in the 2HDM remain the same as in the SM, except with Φ_2 taking the place of the SM Higgs doublet and coupling to the fermions. After electroweak symmetry breaking, the Higgs doublets can be parametrised in terms of the physical scalar degrees of freedom as follows [71]:

$$\Phi_1 = \begin{pmatrix} -H^+ \sin \beta + G^+ \cos \beta \\ \frac{1}{\sqrt{2}}(v \cos \beta - h \sin \alpha + H \cos \alpha - iA \sin \beta + iG^0 \cos \beta) \end{pmatrix}, \quad (2.1)$$

$$\Phi_2 = \begin{pmatrix} H^+ \cos \beta + G^+ \sin \beta \\ \frac{1}{\sqrt{2}}(v \sin \beta + h \cos \alpha + H \sin \alpha + iA \cos \beta + iG^0 \sin \beta) \end{pmatrix}. \quad (2.2)$$

Here, h denotes the SM-like Higgs boson and is a CP-even scalar, accompanied by the conventionally heavier CP-even state H . The field A is the neutral CP-odd pseudoscalar, which we later associate with the 95 GeV resonance.

The H^\pm are a pair of charged Higgs bosons, while G^\pm and G^0 are the Goldstone bosons. The SM Higgs vacuum expectation value (VEV) is $v = 246$ GeV. The VEVs of the two doublets, v_1 and v_2 , are constrained by the requirement that $v_1^2 + v_2^2 = v^2$, and the angle β is defined via $\tan \beta = v_2/v_1$. The angle α diagonalises the CP-even scalar mass matrix and determines the physical mass eigenstates [72].

We can define a new angle $\delta = \beta - \alpha - \pi/2$ to relate the tree-level couplings between the physical resonances and the fermions,

$$c_f^h = \frac{\cos \alpha}{\sin \beta} = \cos \delta - \frac{\sin \delta}{\tan \beta}, \quad c_f^H = \frac{\sin \alpha}{\sin \beta} = -\sin \delta - \frac{\cos \delta}{\tan \beta}, \quad c_u^{A^0} = -c_{d,l}^{A^0} = \cot \beta, \quad (2.3)$$

as well as gauge bosons,

$$c_V^h = \sin(\beta - \alpha) = \sin \delta, \quad c_V^H = \cos(\beta - \alpha) = -\sin \delta \quad (2.4)$$

where $V = W, Z$.

The couplings of the light Higgs boson h approach their SM values ($c_f^h \rightarrow 1$) in the limit $\alpha \rightarrow 0$ and $\beta \rightarrow \pi/2$. In contrast, the heavier scalar H does not couple to fermions at $\alpha = 0$, and decouples from gauge bosons when $\alpha = \beta \pm \pi/2$. The latter condition corresponds to $\cos(\beta - \alpha) = 0$, known as the *alignment limit* of the model. In this limit, the light Higgs h has the same tree-level couplings to the gauge bosons as in the SM.

The tree-level potential for the Type I 2HDM is as follows:

$$V_H = m_{11}^2 \Phi_1^\dagger \Phi_1 + m_{22}^2 \Phi_2^\dagger \Phi_2 - m_{12}^2 (\Phi_1^\dagger \Phi_2 + \text{h.c.}) + \lambda_1 (\Phi_1^\dagger \Phi_1)^2 + \lambda_2 (\Phi_2^\dagger \Phi_2)^2 + \lambda_3 (\Phi_1^\dagger \Phi_1) (\Phi_2^\dagger \Phi_2) + \lambda_4 (\Phi_1^\dagger \Phi_2) (\Phi_2^\dagger \Phi_1) + \frac{\lambda_5}{2} [(\Phi_1^\dagger \Phi_2)^2 + \text{h.c.}], \quad (2.5)$$

where m_{11} and m_{22} are the masses of the doublets, m_{12} is the mixing parameter, and $\lambda_1 \dots, \lambda_5$ are quartic couplings. A fuller treatment of the potential would allow for the additional terms

$$V_H \supset (\lambda_6 \Phi_1^\dagger \Phi_1 + \lambda_7 \Phi_2^\dagger \Phi_2) \Phi_1^\dagger \Phi_2 + \text{h.c.}, \quad (2.6)$$

however, these terms would not be permitted in the \mathbb{Z}_2 symmetry, setting $\lambda_6, \lambda_7 = 0$. This softly broken symmetry is desired as the non-observation of interactions that change fermion flavour without inducing flavour changing neutral currents (FCNCs) requires that the fermions be coupled to a single Higgs doublet only, as mentioned before. This is only possible with the doublets and the fermions being charged under the \mathbb{Z}_2 symmetry, thus forbidding the λ_6, λ_7 terms [73–76]. m_{12}^2 is permitted to be non-zero, softly breaking the \mathbb{Z}_2 symmetry [73, 76].

In the 2HDM, the background fields ϕ_i are identified as the second, real components of the two Higgs doublets respectively,

$$\Phi_i \rightarrow \frac{1}{\sqrt{2}} \phi_i \delta_{n,2} + \Phi_i, \quad (2.7)$$

where n is the component index of the n -tuple. After the two Higgs doublets take these background field values, we arrive at the scalar mass matrix for the fields $\{W, Z, H, A, H^\pm, h, G^0, G^\pm\}$:

$$M^2 = \begin{pmatrix} M_{11}^2 & 0 & 0 & 0 & M_{15}^2 & 0 & 0 & 0 \\ 0 & M_{22}^2 & 0 & 0 & 0 & M_{26}^2 & 0 & 0 \\ 0 & 0 & M_{33}^2 & 0 & 0 & 0 & M_{37}^2 & 0 \\ 0 & 0 & 0 & M_{44}^2 & 0 & 0 & 0 & M_{48}^2 \\ M_{15}^2 & 0 & 0 & 0 & M_{55}^2 & 0 & 0 & 0 \\ 0 & M_{26}^2 & 0 & 0 & 0 & M_{66}^2 & 0 & 0 \\ 0 & 0 & M_{37}^2 & 0 & 0 & 0 & M_{77}^2 & 0 \\ 0 & 0 & 0 & M_{48}^2 & 0 & 0 & 0 & M_{88}^2 \end{pmatrix}, \quad (2.8)$$

where,

$$\begin{aligned}
M_{11}^2 &= m_{11}^2 + \frac{1}{2}(2\lambda_1\phi_1^2 + \lambda_-\phi_2^2), & M_{22}^2 &= m_{11}^2 + \frac{1}{2}(2\lambda_1\phi_1^2 + \lambda_3\phi_2^2), \\
M_{33}^2 &= m_{11}^2 + \frac{1}{2}(6\lambda_1\phi_1^2 + \lambda_+\phi_2^2), & M_{44}^2 &= M_{22}^2, \\
M_{55}^2 &= m_{22}^2 + \frac{1}{2}(2\lambda_2\phi_2^2 + \lambda_-\phi_1^2), & M_{66}^2 &= m_{22}^2 + \frac{1}{2}(2\lambda_2\phi_2^2 + \lambda_3\phi_1^2), \\
M_{77}^2 &= m_{22}^2 + \frac{1}{2}(6\lambda_2\phi_2^2 + \lambda_+\phi_1^2), & M_{88}^2 &= M_{66}^2, \\
M_{15}^2 &= -m_{12}^2 + \lambda_5\phi_1\phi_2, & M_{26}^2 &= -m_{12}^2 + \frac{1}{2}(\lambda_4 + \lambda_5)\phi_1\phi_2, \\
M_{37}^2 &= -m_{12}^2 + \lambda_+\phi_1\phi_2, & M_{48}^2 &= M_{26}^2,
\end{aligned} \tag{2.9}$$

and where we used the abbreviation $\lambda_{\pm} = \lambda_3 + \lambda_4 \pm \lambda_5$. To obtain the final mass eigenvalues, the diagonalisation of the mass matrix in eq. (2.8) is conducted as in [45, 46].

In practice, we wish to calculate the Lagrangian parameters $m_{11}^2, m_{22}^2, m_{12}^2, \lambda_1 \dots, \lambda_5$ from the physical mass inputs $\{m_h, m_H, m_A, m_{H^\pm}\}$, along with the input model angles α, β and the input parameter m_{12} . Appendix B.2 in ref. [46], features the tree-level relations to calculate the Lagrangian parameters, however for a more accurate analysis the one-loop renormalised parameters should be utilised instead. We describe the procedure of vacuum renormalisation in detail in sec. 4.3 below and the appendix A.2.

3. The 2HDM thermal potential

To compute the temperature-dependent effective potential for the Type I 2HDM, we make use of high-temperature dimensional reduction, initially devised in [30, 31, 77–81]. In the context of Lorentz scalar-driven transitions, this approach is well-suited for the high-temperature regime relevant to the transitions we study. Dimensional reduction constructs an effective field theory (EFT) for the static modes at finite temperature and systematically incorporates thermal resummation to all orders. In particular, this method allows for a consistent inclusion of all large thermal corrections including two-loop thermal masses essential for the renormalization scale independence [82–84] which in turn is essential for theoretical consistency and ensuring physically meaningful results, but commonly not achieved, cf. e.g. [38, 85–87].

As an EFT framework, dimensional reduction utilises the thermal hierarchy of scales

$$\frac{g^2}{\pi}T \ll gT \ll \pi T. \tag{3.1}$$

The scale $|p| \sim \pi T$ corresponds to the *hard* non-zero bosonic(fermionic) Matsubara modes [88], $|p| \sim gT \sim m_D$ to the *soft* Debye screening modes, and $|p| \sim g^2T$ to the non-perturbative *ultrasoft* modes in the infrared (IR) [89]. By successively integrating out ultraviolet (UV)

modes—see e.g. [90]—one obtains a sequence of dimensionally reduced EFTs. The final step yields a 3D EFT at the scale of bubble nucleation corresponding to $g^2T/\pi \ll |p| \ll gT$ [91], the so-called *softer* scale [84, 92]. Since in practice, the mass of the phase-transition undergoing scalar will be parametrically larger than the softer scale and therefore the actual EFT lies between the soft and the softer scale. In this final EFT¹, the long-distance dynamics of the transition is encoded in three spatial dimensions.

To compute the thermodynamics of a phase transition, one typically makes use of the effective potential at finite temperature. This potential is then computed in the final 3D EFT at the softer scale. To obtain the potential and the 3D EFT Lagrangian in practice, we utilise the thermal EFT matching software `DRalgo` [93] which we crosscheck via further in-house software in `FORM` [94] and applied `qgraph` [95] for diagram generation.

3.1. The dimensionally reduced effective potential

The starting point for our analysis is the effective potential up to two-loop level in the softer 3D EFT. This corresponds to the functionalities of `DRalgo v1.2.0`. Since we are interested in tracking the phases in multi-field space (cf. sec. 5), we refrain from integrating out further, potentially heavy vector fields [92]. By keeping the matching relations (which relate Lagrangian parameters between the hard, soft, and softer theories) at two-loop level, the options to compute the effective potential amount to its different loop orders, *viz.*

$$[3D@NLO V_3@LO]: \quad \text{two-loop EFT matching,} \quad \text{one-loop effective potential,} \quad (3.2)$$

$$[3D@NLO V_3@NLO]: \quad \text{two-loop EFT matching,} \quad \text{two-loop effective potential.} \quad (3.3)$$

Here, we will focus on the former, namely `[3D@NLO V_3@LO]`. The reason for this is that the direct computation of the two-loop effective potential contains scalar contributions that, for some parts of the parameter space, should be counted as higher-order in comparison to the heavy vector contributions; see [96, 97]. An artefact of this setup is the presence of logarithmically divergent terms in the two-loop potential, which are the result of negative mass eigenvalues in the logarithms coming mostly from sunset diagrams. The divergences lead to numerical issues when calculating the transitions; unphysical vacua are identified due to sharp discontinuous local minima, leading to unphysical phase transition strength parameters (such as bubble walls moving super-luminously, $v_w > 1$). To avoid such issues we follow [98] and compute the one-loop potential with two loop matching relations; see also [84] for a similar application. In the following, we refer to the setup (3.2) as the *two-loop improved one-loop potential*.

The final effective potential at the transition scale, is a function of the 3D effective fields $\phi^{3D} = \{\phi_1^{3D}, \phi_2^{3D}\}$ ² and the temperature T .

¹In Appendix A.1, we discuss the choice of the scale for $\bar{\mu}_{3US}$ which defines the softer scale.

²These background fields are the 3D analogues of the background fields defined in eq. (2.7).

The 4D effective thermal potential, V_4 , can be calculated from the 3D potential via

$$V_4(\phi, T) = TV_3(\phi^{3D}, T) \quad (3.4)$$

using the relation between field values in three- and four-dimensions $\phi^{3D} \rightarrow \phi T^{-\frac{1}{2}}$. Henceforth, we suppress the 3D superscript for the fields in the 3D EFT.

3.2. Higher-orders in the effective potential

In the effective potential at the softer scale, we utilise the NLO matching relations from `DRalgo` directly, based on the example file `2hdm.m`.³ Similar matching relations can also be found in [46].⁴ For the corresponding vacuum renormalisation, see secs. 4.3 and A.2.

Up to two-loop order, the 3D effective potential is

$$V_3 = V_{0,3} + V_{1,3} + V_{2,3}, \quad (3.5)$$

$$V_{1,3} = \sum_i n_i J_3(\bar{m}_i^2(\phi, T)), \quad (3.6)$$

where $d = 3 - 2\epsilon$, $V_{0,3}(\phi, T)$ is the three-dimensional version of the tree-level potential (2.5) [45, 46], and the degrees of freedom, n_i , are d -dependent. The corresponding mass eigenvalues \bar{m}_i of the dynamical fields $i \in \{W, Z, H, A, H^\pm, h, G^0, G^\pm\}$ in the 3D EFT depend on the background fields for the two Higgs doublets, whose 4D analogues are seen in eq. (2.1). We discussed the calculation of the mass eigenvalues from the mass matrix in sec. 2.

Similarly, to the 4D vacuum case and the corresponding Coleman-Weinberg potential [99], the one-loop 3D EFT potential, $V_{1,3}$, takes a closed form. The corresponding integrals are UV-finite and three-dimensional

$$J_3(m^2) = \frac{1}{2} \int_{\mathbf{p}} \ln(p^2 + m^2) \stackrel{d=3-2\epsilon}{=} -\frac{1}{12\pi} [m^2]^{\frac{3}{2}}. \quad (3.7)$$

The two-loop contributions, $V_{2,3}$, to the potential (3.5), as well as the two-loop 3D EFT matching relations are directly adopted from `DRalgo` [93] can also be taken from [100]. The parameters of this final 3D EFT are evolved to the 3D renormalisation group (RG) scale, $\bar{\mu}_3$, which we set to $\bar{\mu}_3 = T$ in our analysis. The RG evolution and vacuum renormalisation procedures are detailed in secs. 4.3 and A.2.

In sec. 3.1, we argued that directly employing the two-loop effective potential, without integrating out heavy vector and temporal modes to induce the transition, can lead to pathological behaviour for some benchmark points along the transition path in the multi-field field space.

³See the `DRalgo` GitHub, <https://github.com/DR-algo/DRalgo/blob/main/examples/2hdm.m>.

⁴In comparison with the matching relations of [46], scalar masses in our softer-scale matching relations are counted as higher-order inside of logarithmic terms for e.g. \bar{m}_{11}^2 . Also, in eq. (3.15) of [46], N_f should be the number of fermions and not the number of families.

Since the preferred approach is therefore to use the [3D@NLO $V_{\text{eff}}@L0$] prescription (3.2), one may wonder about the importance of omitting two-loop corrections in the effective potential while keeping them in the matching. These effects have been studied in [84, 98], which concluded that the dominant uncertainties are associated with higher-order corrections in the matching. To investigate this and support our choice of using the setup (3.3) for our scan, in sec. 5 we examine a few benchmark points to assess the magnitude of uncertainty introduced by neglecting higher-order terms in the effective potential. These benchmark points are summarised in table 2.

4. Bubble Nucleation and Gravitational Waves

To find the phases, calculate phase transition properties and gravitational wave spectra from our 4D potential, we use the `PhaseTracer2` package for C++ [101, 102]. The package automates the pipeline from a 4D thermal potential to the gravitational wave spectrum parameters and signal-to-noise ratios (SNRs) for proposed gravitational wave interferometers, such as LISA [62, 103] and Taiji [65]. In this section, we provide a brief review of the computation performed by the package.

4.1. Bubble nucleation

First order phase transitions occur through bubble nucleation, which describe tunnelling from a high temperature phase (typically symmetric under a symmetry) to a low temperature phase, which are separated by a potential barrier.

Bubbles nucleate when there is a viable transition path between the minima with a low enough action. After switching to Euclidean space, with $t \rightarrow -i\tau$, the transition path can be parametrised as $\phi_1(\rho)$ and $\phi_2(\rho)$ with $\rho = \sqrt{\tau^2 + \mathbf{x}^2}$ being a radial parameter in space, indicating a spherically symmetric bubble. The associated Euclidean action can be written as

$$S_d[\phi_1, \phi_2](T) = \Omega_{d-1} \int_0^\infty \rho^{d-1} \left\{ \frac{1}{2}(\dot{\phi}_1^2 + \dot{\phi}_2^2) + V(\phi_1, \phi_2, T) \right\} d\rho, \quad (4.1)$$

with d being the number of dimensions of the $O(d)$ -symmetric field configuration, here $d = 3$ for nucleation by thermal fluctuations. The Euler-Lagrange equation provides the saddle point of this action, known as the bounce equation, given by [104]

$$\ddot{\phi}_i(\rho) + \frac{d-1}{\rho} \dot{\phi}_i(\rho) = \frac{\partial}{\partial \phi_i} V(\phi_1, \phi_2, T). \quad (4.2)$$

This equation is solved with the boundary conditions $\dot{\phi}_i(0) = \dot{\phi}_i(\rho \rightarrow \infty) = 0$, and $\phi_i(\rho \rightarrow \infty) = \phi_i^f$, where ϕ_i^f is the value of the fields at the true vacuum (see [105, 106] for a discussion of the appropriate boundary conditions for tunneling). In our two-field model, we employ

PhaseTracer2 [102] to calculate the bounce configuration using the path deformation method, where an initial guess for the path is perturbed using normal forces to minimise the bounce action. The action $S_3(T)$ is then calculated for the bounce solution at temperature T .

We define the onset of the phase transition through the following nucleation criterion [61, 107, 108]

$$\frac{S_3}{T_n} \simeq 141 + \ln \frac{A}{T_n^4} - 4 \ln \frac{T_n}{100 \text{ GeV}} - \ln \frac{\bar{\beta}}{100 H_*}, \quad (4.3)$$

which defines the nucleation temperature T_n . While this condition is phrased in terms of the Euclidean action, it is derived from the requirement that the nucleation rate per unit volume becomes significant in an expanding universe. More precisely, it approximates the point at which the probability of bubble nucleation in a Hubble volume becomes order unity. The full percolation criterion requires integrating the nucleation rate over spacetime to track the volume fraction of the false vacuum (see e.g. [109]), which is well approximated by the above condition in most cases. Here

$$\bar{\beta} = \left. \frac{d(S_3/T)}{dt} \right|_{t=t_*} = H_* T_* \left. \frac{d(S_3/T)}{dT} \right|_{T=T_*}. \quad (4.4)$$

is a measure of the inverse time it takes for the phase transition to complete, where H_* (T_*) refers to the Hubble constant (temperature) at the time t_* .⁵ The percolation temperature, T_p , can be calculated by using the percolation criterion [110], which is

$$\frac{S_3}{T_p} \simeq 131 + \ln \frac{A}{T_p^4} - 4 \ln \frac{T_p}{100 \text{ GeV}} - 4 \ln \frac{\bar{\beta}}{100 H_*} + 3 \ln v_w, \quad (4.5)$$

where in our numerical studies we use an ansatz for $\bar{\beta}/H_* = 10^4$, justified a posteriori in sec. 5. For the EWPT, $\ln(A/T^4) \simeq -14$ [111].⁶ A thorough calculation of v_w can be achieved through hydrodynamical simulations of the phase transition, as in refs. [114, 115], however these are time consuming and v_w is typically supplied as an input parameter [102, 116]. A general perturbative determination of v_w requires including out-of-equilibrium effects [117] as recently automated in [118]. It has been argued by [119] that v_w can be approximated by the Chapman-Jouguet velocity, typically used to describe explosive detonations:

$$v_w \approx v_{\text{CJ}} = \frac{1}{1 + \bar{\alpha}} \left(c_s + \sqrt{\bar{\alpha}^2 + \frac{2}{3} \bar{\alpha}} \right), \quad (4.6)$$

⁵Note that we have added a bar to the conventional notation to avoid confusion with the Lagrangian parameter in the 2HDM.

⁶In practice, the nucleation rate receives higher-order corrections from fluctuations around the bounce solution, modifying the prefactor $A(T)$ and the interpretation of S_3 , and have recently been studied in detail using functional determinant methods [91, 112]. Public tools such as `bubbleDet` [113] enable the automated inclusion of these corrections, providing a more accurate estimate of the nucleation rate.

where we take the speed of sound in the plasma to be $c_s = 1/\sqrt{3}$. The parameter $\bar{\alpha}$ characterises the strength of the phase transition and will be defined below. For the strongest transitions we find in sec. 5 (which have $\bar{\alpha} \approx 4 \times 10^{-3}$), the Chapman-Jouguet velocity gives $v_w \approx 0.63$. We use this value as an input to (4.5) in our numerical studies. However, (4.6) is valid only in a restricted regime. As noted in [116, 120], the assumptions underlying the CJ condition do not strictly apply to cosmological phase transitions. More accurate treatments bracket the true value of v_w between two physical limits: a ballistic limit, representing minimal interaction between the bubble wall and plasma [116], and a local thermal equilibrium (LTE) limit, which assumes local entropy conservation and requires detailed thermodynamic input [121, 122]. The LTE expression has been shown to match well with numerical simulations [123], but is computationally prohibitive for parameter scans. For simplicity, we adopt the Chapman–Jouguet approximation in this work.

The trace anomaly difference of the energy-momentum tensor,

$$\Delta\theta = \left(V(\phi, T_*) - \frac{T_*}{4} \frac{\partial}{\partial T} V(\phi, T) \Big|_{T_*} \right) \Big|_{\phi_t}^{\phi_f}, \quad (4.7)$$

is taken in the relativistic plasma limit and in practice receives further corrections if the broken-phase speed of sound squared differs from $c_s^2 = 1/3$ [124, 125]. Here, T_* is the gravitational wave production temperature, typically identified with the percolation temperature of the phase transition T_p . $\Delta\theta$ quantifies the amount of energy available for conversion to space-time shear stress, which is represented by the off-diagonal components of the stress-energy tensor $T^{\mu\nu}$, and is responsible for the generation of gravitational waves [126, 127].

The ratio of the trace anomaly difference to the energy density in the plasma (approximated by the radiation energy density at the GW production temperature, $\rho_r = \pi^2 g_* T_p^4/30$), quantifies the energy available for gravitational wave production, and thus characterises the strength of the phase transition:⁷

$$\bar{\alpha} \equiv \frac{\Delta\theta}{\rho_r}. \quad (4.8)$$

Several alternative definitions of $\bar{\alpha}$ exist in the literature. A commonly used one defines it as the ratio of vacuum energy difference to the radiation energy density, $\bar{\alpha} = \Delta V_{\text{eff}}/\rho_r$, which neglects thermal effects [60]. Another popular definition comes from hydrodynamics, where $\bar{\alpha} = \Delta\rho/w$, with $w = \rho + p$, describing the energy injected into the plasma relative to its enthalpy [128]. A third definition is based on the *pseudo* trace anomaly definition [129], which approximates the energy available for shear stress using a simplified thermal treatment. The definition used in this work includes both vacuum and thermal contributions and is particularly appropriate for models like the 2HDM, where no tree-level barrier is present and thermal corrections are essential for realizing a first-order phase transition (FOPT).

⁷As above, we use barred notation for this parameter to differentiate it from the Lagrangian parameters in the 2HDM.

4.2. Gravitational Wave spectrum

Early universe FOPTs give three main sources of gravitational waves: sound waves induced by the expansion of bubbles into the surrounding plasma, bubble collisions creating anisotropic stress directly [130], and turbulence in the plasma [131, 132] caused by bubble collision energy. Typically, the GW contributions from these three sources can be calculated from knowledge of the thermal parameters $\bar{\alpha}$, $\bar{\beta}/H_*$ and v_w . In our case, the sound wave contribution dominates throughout our parameter space, and we will therefore limit our discussion to this effect.

Numerical simulations indicate that sound waves are typically the dominant source of GWs from FOPTs [133, 134] (however, see [135] for examples of exceptions). Two length scales dictate the bounds of the power spectrum of the acoustic GW contribution, which are the mean distance between the bubbles [61] (cf. [110]),

$$R_* = (8\pi)^{1/3} v_w / \bar{\beta}, \quad (4.9)$$

and the thickness of the expanding sound shell in the plasma outside the bubble of the new phase,

$$\Delta R_* = R_* \frac{|v_w - c_s|}{c_s}. \quad (4.10)$$

The sound shell thickness ΔR_* dictates the position of the peak of the power spectrum [136].

An analytic fitting formula for the acoustic GW contribution was derived in [61, 134, 136], which we write here in the form used by `PhaseTracer2` [102],

$$\Omega_{\text{sw}} h^2(f) = 2.061 F_{\text{gw},0} \Gamma^2 \bar{U}_f^4 S_{\text{sw}}(f/f_{\text{sw}}) \tilde{\Omega}_{\text{gw}} \times \min(H_* R_* / \bar{U}_f, 1) (H_* R_*) h^2, \quad (4.11)$$

where $\min(H_* R_* / \bar{U}_f, 1) (H_* R_*)$ accounts for the finite lifetime of the source. Here,

$$F_{\text{gw},0} = 3.57 \times 10^{-5} \left(\frac{100}{g_*} \right)^{1/3}, \quad (4.12)$$

$$S_{\text{sw}}(x) = x^3 \left(\frac{7}{4 + 3x^2} \right)^{7/2}, \quad (4.13)$$

with $S_{\text{sw}}(f)$ being the spectral shape the peak frequency of the sound waves

$$\frac{f_{\text{sw}}}{1 \mu\text{Hz}} = \frac{2.6}{H_* R_*} \left(\frac{z_p}{10} \right) \left(\frac{T_*}{100 \text{ GeV}} \right) \left(\frac{g_*}{100} \right)^{1/6}. \quad (4.14)$$

Γ is the ratio of enthalpy to the energy density of the plasma, taken to be 4/3 for the early universe, \bar{U}_f is the enthalpy weighted root mean square fluid velocity of the plasma, and $z_p \sim 10$ and $\tilde{\Omega}_{\text{gw}} \sim 0.012$ are parameters informed by the numerical simulations. Thus, we see that $\Gamma \bar{U}_f^2 = K_{\text{sw}}$ is the ratio of kinetic energy in the fluid to its energy density. We can write this as

$$\Gamma \bar{U}_f^2 = K_{\text{sw}} = \frac{\kappa_{\text{sw}} \bar{\alpha}}{1 + \bar{\alpha}}, \quad (4.15)$$

where κ_{sw} is an efficiency factor for the conversion of the latent energy of the phase transition into the acoustic kinetic energy of the fluid. `PhaseTracer2` employs the following fitting formula for κ_{sw} when the wall velocity is taken to be the Chapman-Jouguet velocity:

$$\kappa_{\text{sw}} = \frac{\sqrt{\bar{\alpha}}}{0.135 + \sqrt{0.98 + \bar{\alpha}}}. \quad (4.16)$$

The signal to noise ratios (SNRs) for GW experiments such as LISA can be calculated through [61, 137]

$$\text{SNR}_{\text{LISA}} = \sqrt{\mathcal{T} \int_{f_{\text{min}}}^{f_{\text{max}}} df \left(\frac{h^2 \Omega_{\text{gw}}(f)}{h^2 \Omega_{\text{sens}}(f)} \right)^2}, \quad (4.17)$$

where \mathcal{T} is the length of time for data collection, and $h^2 \Omega_{\text{sens}}(f)$ is the frequency dependent sensitivity of the experiment. It is given by [137]

$$h^2 \Omega_{\text{sens}}(f) = \frac{4\pi^2}{3H_0^2} f^3 S_h(f) \quad (4.18)$$

where the $S_h(f)$ is the inverse noise weighted sensitivity to the spectral density,

$$S_h(f) \simeq \frac{20\sqrt{2}}{3} \left(\frac{S_I(f)}{(2\pi f)^4} + S_{II}(f) \right) \left(1 + \left(\frac{3f}{4f_*} \right)^2 \right). \quad (4.19)$$

For LISA, the term involving

$$S_I(f) = 5.76 \times 10^{-48} \left(1 + \left(\frac{f_1}{f} \right)^2 \right) \text{Hz}^3 \quad (4.20)$$

where $f_1 = 0.4 \text{ mHz}$, gives the acceleration noise associated with spurious forces on the test masses, for example those that occur due to the build up of electrostatic charge [138]. The term involving

$$S_{II}(f) = 3.6 \times 10^{-41} \text{Hz}^{-1} \quad (4.21)$$

corresponds to the noise from optical path length fluctuations. The characteristic LISA frequency $f_* = c/(2\pi L)$, where $L = 2.5 \times 10^6 \text{ km}$ and c is the speed of light, relates to the distance that light travels between LISA sensors. Useful quantities that can be taken from $\Omega_{\text{gw}} h^2$ include the frequency f_{gw} for which the amplitude is greatest (the ‘peak frequency’), and the peak amplitude $\Omega_{\text{gw}} h^2(f_{\text{gw}})$ at that frequency.

4.3. From dimensionally reduced potential to gravitational waves

In the previous two sections, we have described our calculation of the 2HDM thermal potential and the dynamics of the first order phase transition with a light degree of freedom. We summarise the calculation pipeline with the following steps:

1. First, we take the physical input parameters $\{m_h, m_H, m_A, m_{H^\pm}, \tan(\beta), \cos(\beta-\alpha), m_{12}\}$ defined at the input RG scale $\Lambda_0 = m_Z$.
2. Next, we use these physical input parameters to calculate the one-loop renormalised 4D Lagrangian input parameters $\{m_{11}^2, m_{22}^2, m_{12}^2, \lambda_1, \dots, \lambda_5, y_t, g_{1-3}^2\}$, see also appendix A.2.
3. Next, we use the beta functions (provided in appendix A.1) to RG-evolve these renormalised 4D Lagrangian parameters to the matching scale $\bar{\mu}_4 = 4\pi e^{-7E} T$, such that we have $\{\bar{m}_{11}^2, \bar{m}_{22}^2, \bar{m}_{12}^2, \bar{\lambda}_1, \dots, \bar{\lambda}_5, \bar{y}_t, \bar{g}_{1-3}^2\}$.

4. Using the soft 3D matching relations, we calculate the soft parameters

$$\left\{ (m_{11}^{3D})^2, (m_{22}^{3D})^2, (m_{12}^{3D})^2, \lambda_1^{3D}, \dots, \lambda_7^{3D}, y_t^{3D}, (g_1^{3D})^2, \dots, (g_3^{3D})^2 \right\} \quad (4.22)$$

at the scale $\bar{\mu}_3 = T$. In the soft theory, $\lambda_{6,7}^{3D}$ arise from integrating out the non-zero Matsubara modes, despite our model having as input $\lambda_{6,7} = 0$.

5. Using the softer matching relations, we calculate the softer parameters

$$\left\{ (\bar{m}_{11}^{3D})^2, (\bar{m}_{22}^{3D})^2, (\bar{m}_{12}^{3D})^2, \bar{\lambda}_1^{3D}, \dots, \bar{\lambda}_7^{3D}, \bar{y}_t^{3D}, (\bar{g}_1^{3D})^2, \dots, (\bar{g}_3^{3D})^2 \right\} \quad (4.23)$$

at the softer matching scale $\bar{\mu}_{3US} = \bar{\mu}_3$.

6. The softer parameters are input to construct the 3D effective potential, $V_3(\phi_1^{3D}, \phi_2^{3D}, T)$. As mentioned previously, we find the 4D effective potential $V_4(\phi_1, \phi_2, T)$ through eq. (3.4).
7. Through $V_4(\phi_1, \phi_2, T)$, we can then,
 - (a) Find the minima of the potential, identifying when they co-exist and finding possible critical temperatures T_c .
 - (b) Find possible transition paths between the minima and calculate the action S along the paths, comparing S/T to the percolation criterion in (4.5). This allows us to calculate the percolation temperature(s) T_p .
 - (c) Calculate the transition parameters $\bar{\alpha}, \bar{\beta}/H_*$, and then the peak gravitational wave frequencies and amplitudes associated with the transitions. From this, the signal-to-noise ratios (SNRs) for LISA or other experiments can be calculated.

5. Parameter scans

As explained above, we work in the real 2HDM Type I, associating the 95 GeV resonance with the pseudoscalar A . The model features eight free parameters, of which we fix six to

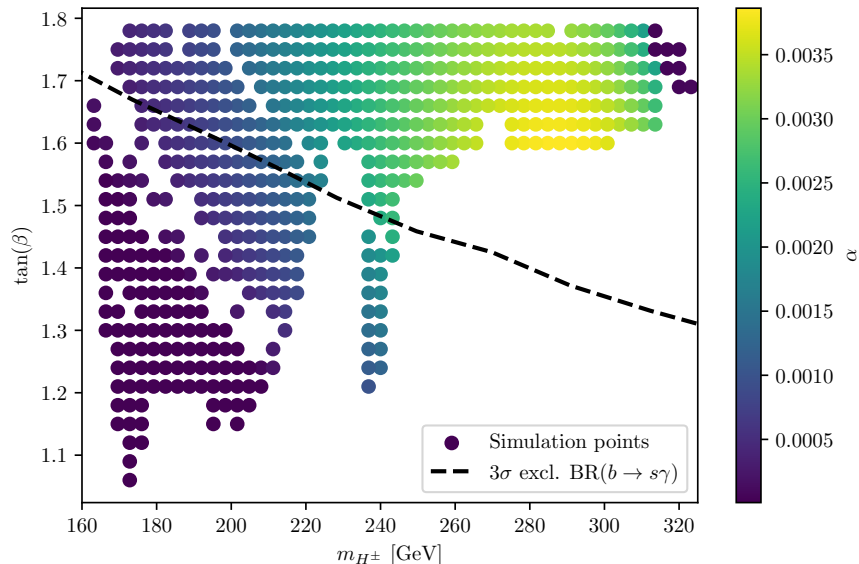


Figure 1: Computed phase transitions with a light pseudoscalar $m_A = 95$ GeV in the region seen in fig. 5 of ref. [25]. We have fixed $m_H = 160$ GeV and $\cos(\beta - \alpha) = -0.2$, with the other fixed values as in tab.1.

benchmark values informed by theoretical and experimental constraints (tab. 1). In particular, we fix $\tan\beta$ to be within the range necessary to fit both the diphoton signal and the ditau signal (see e.g. ref. [25]). Interestingly, we have confirmed that the value of $\tan\beta$ chosen here also optimises the strength of the EWPT as can be seen in fig. 1. In this figure, we show the latent heat parameter α in the parameter space allowed by current constraints [25], fixing $m_H = 160$ GeV and $\cos(\beta - \alpha) = -0.2$ which will be motivated a posteriori. From this result it is seen that the value of $\tan\beta$ chosen to fit both collider signals also leads to stronger phase transitions, when $m_{H^\pm} \approx 290$ GeV. This also partially alleviates the tensions with flavour physics ($b \rightarrow s\gamma$).

Lastly, we find little sensitivity to m_{12} below $m_{12} \sim 10$ GeV, and fix it at an arbitrary value of $m_{12} = 1$ GeV to represent that entire range. A preliminary scan in m_{12} up to 10^2 GeV showed that $\bar{\alpha}$ was strongest for $m_{12} \approx 10^{1.35}$ GeV. An analysis with m_{12} fixed to this value showed no qualitative and only minor quantitative differences from the conclusions presented below (maximum SNR at LISA was found to be $\mathcal{O}(10^{-6})$).

For supercooled transitions, it is also important to check that volume of space that is in the false vacuum is decreasing, along with checking the percolation condition (4.5). This is because the condition can be met and yet the progression of the transition could be reversed. Since supercooling as quantified by the relative difference of $\delta_{\text{SC}} = (T_c - T_n)/T_n$ is never larger than $\sim 20\%$ across the parameter space, the transitions are not strongly supercooled. Due to

Parameter	Value	Motivation
m_A	95 GeV	Resonance mass
m_h	125 GeV	SM-like Higgs
m_{H^\pm}	290 GeV	Alleviate $b \rightarrow s\gamma$ tension
$\tan\beta$	1.57	Fit $\gamma\gamma$ and $\tau\tau$ excesses
m_{12}^2	1 GeV ²	Minimal impact on EWPT strength
$v = \sqrt{v_1^2 + v_2^2}$	246 GeV	Electroweak VEV

Table 1: Fixed inputs for our scan identifying A, H with the resonance respectively.

the absence of such large supercooling, the condition of shrinking false vacuum is also met for the investigated parameter space and no subsequent thermal inflation is observed [139, 140]. The observed mild values of supercooling result also in relatively small field values (cf. sec. 5) and no large separation of temperature scales in contrast to classically conformal models, where supercooling is large and one needs to utilise a more refined framework [141–143]. In turn, this gives credence to the validity of the high-temperature expansion for computing both the transition timescale and the strength within the 3D EFT framework. The remaining two parameters are varied as

$$\cos(\beta - \alpha) \in [-0.3, 0.3], \quad m_H \in [130, 300] \text{ GeV}. \quad (5.1)$$

We vary the temperature T between 300 and 20 GeV. As we shall see, we do not expect that allowing for smaller m_H in our scan leads to different vacuum structures or stronger transitions.

These ranges are fully compatible with electroweak-precision fits: by keeping $m_H \in [130, 300]$ GeV (with near-degenerate A and H^\pm) and $|\cos(\beta - \alpha)| \leq 0.3$, the S and T parameters lie within the 2σ allowed region of global fits. Moreover, the implied quartic couplings in the scalar potential remain $\mathcal{O}(1)$, well below the tree-level unitarity bounds (and safely perturbative), so all $2 \rightarrow 2$ scalar–scalar amplitudes satisfy $|a_0| < \frac{1}{2}$. We show the results of our scan in Fig. 2. We find that the vacuum structure as a function of temperature depends on $\cos(\beta - \alpha)$ and m_H as follows. For small $m_H \lesssim 200$ GeV and large $\cos(\beta - \alpha) \gtrsim -0.1$, the first vacuum away from the origin to appear does not give the SM-like resonance h a VEV. The further, SM-like vacuum only appears later, and EWSB thus occurs through a two-step transition. Either of these transitions is weaker than the immediate transition to the SM-like vacuum, which occurs for a band of smaller $\cos(\beta - \alpha)$. This is because in this range, the EW gauge bosons couple more strongly to the SM-like state. For lower $\cos(\beta - \alpha)$ the transition again occurs in two steps. For large m_H and $\cos(\beta - \alpha)$, no barriers are created and EWSB occurs via a crossover.

In the second and third panel, we show the peak amplitude and frequency for the GW spectrum resulting from strongest transition. As expected, the largest amplitudes are found

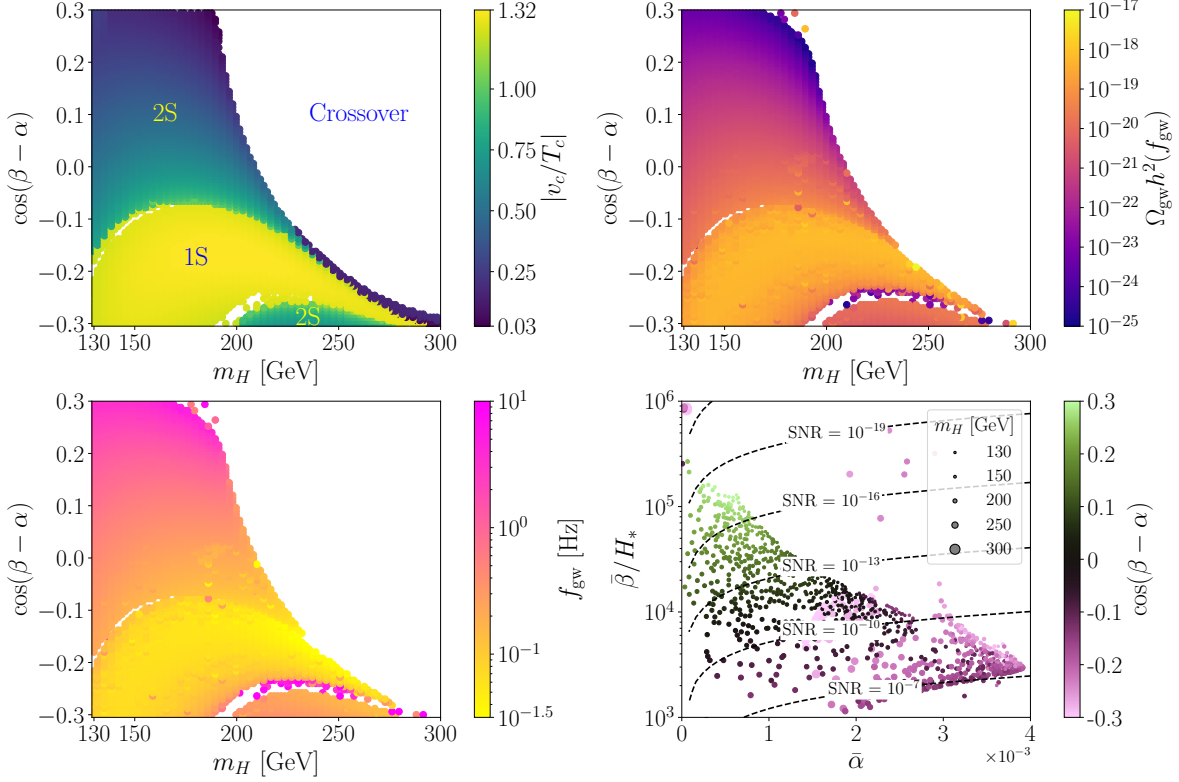


Figure 2: **Top Left Panel:** First order phase transitions in the $m_H - \cos(\beta - \alpha)$ plane, with the colour showing the value of the largest v_c/T_c for that parameter point. Regions of two step (2S) and one step (1S) first order phase transitions are labelled, along with the region that has crossovers. **Top Right Panel:** As for top left, showing the peak amplitude $\Omega_{\text{gw}} h^2(f_{\text{gw}})$ instead. **Bottom Left Panel:** As for top left, showing the peak frequency f_{gw} instead. **Bottom Right Panel:** Computed phase transitions for different parameter points plotted against transition parameters $\bar{\alpha}$ and $\bar{\beta}/H_*$. Only a randomly sampled selection (1 in 4) is chosen to be shown on the plot to make the trends clear. The value of $\cos(\beta - \alpha)$ for each point is shown by the colour, whereas the value of m_H is shown by the size of the circle. We show LISA SNR curves for an ansatz transition temperature of 160 GeV, and an ansatz $v_w = 0.63$.

BM	m_H	$\cos(\beta - \alpha)$	$\bar{\alpha}_{1\text{-loop}}$	$\bar{\alpha}_{2\text{-loop}}$	Error
2S	130	0	0.0017	0.0035	51%
1S	200	-0.2	0.00015	0.00019	21%

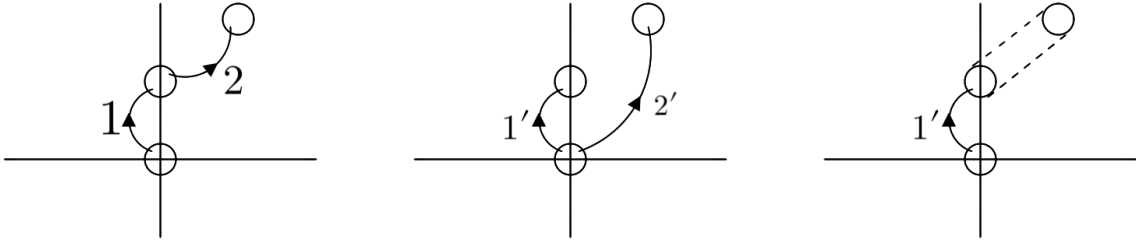
Table 2: The transition strength parameter $\bar{\alpha}$ and relative errors for Benchmarks 2S and 1S at (2-loop improved) 1-loop [3D@NLO V_3 @LO] and 2-loop [3D@NLO V_3 @NLO]. Other parameters are fixed according to Table 1.

in the band where the transition occurs directly. However, the amplitudes throughout this parameter space are lower than can be probed by the anticipated GW experiments in the next decades. Moreover, the peak frequencies are typically outside of the range of space-based interferometers, reflecting the large $\bar{\beta}/H_*$ parameters found in our scan.

This is explicitly demonstrated in the last panel of Fig. 2, in which we show the predicted latent heat parameter $\bar{\alpha}$ and inverse duration parameter $\bar{\beta}/H_*$ for the range of models we scan over. We show contours of fixed SNR for the LISA experiment (calculated through eq. 4.17) with dashed contours, where we assumed a transition temperature of 160 GeV which we found to be characteristic, and a wall speed of $v_w = 0.63$. No models in our scan reach SNR unity.

Finally, we attempt to quantify the error introduced by our use of the two-loop improved one-loop potential instead of the two-loop potential, which we do not use for our parameter scan due to the issues discussed in sec. 3.1. We evaluate two benchmark points which are representative of the two step region (2S) and the one step region (1S), at both one and two loop, making use of the two loop matching relations in both cases.

The results of these benchmark points are found in Table 2. We find that the differences in percolation temperatures are in agreement with the differences between the 1-loop and 2-loop calculations in ref. [47], and that the differences in $\bar{\alpha}$ are of order $\mathcal{O}(0.1 - 1)$. This means that while the 2-loop potential provide important quantitative contributions, the transition strengths are within the same order of magnitude, resulting in similarly weak SNRs. For benchmark 2S, the interim phase appears earlier than the SM-like vacuum, resulting in the 2-step transition (fig. 3a). For benchmark 1S at 1-loop, the single step occurs directly from the origin to the SM-like vacuum (fig. 3b), as the interim phase appears at a colder temperature than the SM-like vacuum, and disappears quickly. For the same benchmark 2-loop, the interim phase and the further SM-like vacuum are not distinct and instead there is a crossover between them. Thus the transition happens to the field space location of the interim phase, and then the phase migrates to the location of the SM-like vacuum (fig. 3c). As higher order corrections are known to change the type of phase transition [144], this is a source of the difference between the 1-loop and 2-loop results. We illustrate this phase structure in fig. 3. For benchmark 1S at 1-loop, we provide the $\bar{\alpha}$ of transition 1' in fig. 3b



(a) Benchmark 2S showing a 2-step transition at both 1- and 2-loop.

(b) Benchmark 1S @ 1-loop, showing a direct transition labelled 2'. A weaker transition 1' (with a lower T_p) is also calculated.

(c) Benchmark 1S @ 2-loop, showing a direct transition labelled 1'. This is followed by a crossover to the zero-temperature minimum.

Figure 3: Illustrative phase diagrams for the benchmark points 1S and 2S in table 2, with regions that contain 1S and 2S shown in fig. 2.

in the table, rather than the stronger transition 2'. This provides a more direct comparison to the 1' transition of 1S at 2-loop (see fig. 3c).

6. Conclusions

In this paper, we identified the available parameter space for the implementation of the 95 GeV resonance into the real Type I 2HDM based on previous work, ensuring a simultaneous best fit for the $b \rightarrow s\gamma$ branching ratio, and the $\gamma\gamma$ and $\tau\tau$ resonances. The constraints leave m_H and $\cos(\beta - \alpha)$ as the parameters that are most free to change. After fixing the rest of the parameters in the model, we use the dimensionally reduced thermal effective potential to compute the transition parameters $\bar{\alpha}$ and $\bar{\beta}/H_*$. We also compute the gravitational wave spectrum $\Omega_{\text{gw}}h^2(f)$, its peak frequency f_{gw} and peak amplitude $\Omega_{\text{gw}}h^2(f_{\text{gw}})$.

We find that in the $m_H - \cos(\beta - \alpha)$ parameter space, there are regions of crossovers, one step, and two step first order transitions. The region with one step transitions predictably provides the strongest transitions, with $\bar{\alpha} \sim 0.0035$. These correspond to peak amplitudes of $\sim 10^{-18}$ and $f_{\text{gw}} \sim 10^{-1.5}$, resulting in the strongest SNRs for the LISA experiment being around 10^{-7} , which are much weaker than the conventionally desired thresholds of $\text{SNR} \sim 10$. We conclude that a model that simultaneously seeks to explain the $\gamma\gamma$, $\tau\tau$ and LEP excesses in the 2HDM could only result in FOPTs that are too weak to be detected by LISA, and would require interferometers with much greater sensitivity to the cHz frequency band.

The modest strength of the EWPT observed in our scan can be attributed to the radiative origin of the barrier separating the vacua. In the parameter space compatible with

identifying the 95 GeV excess as a light pseudoscalar, the scalar mass spectrum is relatively compressed, limiting the enhancement of thermal cubic terms that typically arise from large mass splittings. As a result, the barrier is primarily generated by gauge boson loops, similar to the Standard Model. The light pseudoscalar itself contributes only weakly to the thermal potential at high temperatures, and does not induce a significant enhancement of the barrier. This scenario contrasts with regions of the 2HDM where heavier scalars can radiatively strengthen the transition or where tree-level terms provide a barrier already at zero temperature. In particular, previous studies have shown that large mass splittings, especially between the pseudoscalar and the heavy scalar or charged Higgs, can amplify scalar contributions to the thermal potential and lead to a strong first-order transition. Consequently, while the transition is generically first-order in our setup, it is not sufficiently strong to produce observable gravitational wave signals or support electroweak baryogenesis without additional model ingredients.

Another possibility for generating a large barrier via significant mass splitting is to treat the second, heavier scalar as a UV degree of freedom in the final EFT, and integrate it out during dimensional reduction. However, implementing this approach would require dynamically switching between different EFT hierarchies throughout the parameter scan [92]. We have therefore chosen to focus on the thermal mass hierarchy as outlined in our analysis, and defer the exploration of more intricate EFT hierarchies to future work.

Lastly, we comment on how additional degrees of freedom could alter the thermal history and potentially enhance the strength of the phase transition. In the 2HDM we discussed, the barrier between the high temperature and the low temperature vacuum is generated radiatively. A coupling of the Higgs sector to a scalar gauge singlet can introduce a tree-level barrier in the potential. Alternatively, fermionic extensions or higher-dimensional operators (e.g. $(H^\dagger H)^3/\Lambda^2$) in the UV of the 4D theory [82] can enable viable electroweak baryogenesis. Additionally, higher-dimensional operators in the UV of the 3D EFT theory [145–147] can modify the shape of the potential at finite temperature, and thus the strength of the transition. These extensions may also shift the transition dynamics into a more strongly supercooled regime, lowering the percolation temperature and thus pushing the GW signal into the most sensitive frequency band of space-based interferometers. A systematic exploration of such scenarios within the dimensional reduction framework, including complementary constraints from colliders and electroweak precision studies (e.g. [148, 149]) is a promising direction for future work.

Acknowledgements

We generously thank Lauri Niemi, Tuomas V.I. Tenkanen, and Jorinde van de Vis for illuminating discussions. We also thank the authors of `PhaseTracer2` [101, 102] for their support during the setup of the model parameters scans. AB and DC are supported by the STFC under Grant No. ST/T001011/1. PS was supported by the Swiss National Science Foundation (SNSF) under grant PZ00P2-215997.

A. Renormalisation of the 2HDM

A.1. Running and β -functions

Electroweak resonances are typically measured at the Z -pole, meaning that the physical mass inputs will exist at an energy scale $\mu = m_Z$. Through the one-loop renormalisation relations, we can relate this input to Lagrangian parameters that also exist at the same energy scale. Next, we can renormalisation group evolve the Lagrangian parameters via the beta functions to the 4D scale $\mu = \bar{\mu}_4$ of our theory, where they can then act as input for our model.

The renormalisation group equations listed below are associated with the parameters of the 2HDM and encode their running with respect to the four-dimensional $\overline{\text{MS}}$ renormalisation scale $\bar{\mu}_4$ via the β -functions. To this end, we use

$$t \equiv \ln \bar{\mu}_4, \quad (\text{A.1})$$

where $\bar{\mu}_4^2 \equiv 4\pi e^{-\gamma_E} \mu^2$,⁸ and find at one-loop level:

$$\partial_t g_1^2 = \frac{7}{8\pi^2} g_1^4, \quad (\text{A.2})$$

$$\partial_t g_2^2 = -\frac{3}{8\pi^2} g_2^4, \quad (\text{A.3})$$

$$\partial_t g_3^2 = -\frac{7}{8\pi^2} g_3^4, \quad (\text{A.4})$$

$$\partial_t y_t = \frac{1}{192\pi^2} y_t (-17g_1^2 - 27g_2^2 - 96g_3^2 + 54y_t^2), \quad (\text{A.5})$$

$$\partial_t m_{11}^2 = \frac{1}{32\pi^2} (-3m_{11}^2(g_1^2 + 3g_2^2 - 8\lambda_1) + 4m_{22}^2(2\lambda_3 + \lambda_4)), \quad (\text{A.6})$$

$$\partial_t m_{22}^2 = \frac{1}{32\pi^2} (-3m_{22}^2(g_1^2 + 3g_2^2 - 4y_t^2 - 8\lambda_2) + 4m_{11}^2(2\lambda_3 + \lambda_4)), \quad (\text{A.7})$$

$$\partial_t m_{12}^2 = \frac{1}{32\pi^2} m_{12}^2 (-3g_1^2 - 9g_2^2 + 6y_t^2 + 4(\lambda_3 + 2\lambda_4 + 3\lambda_5)), \quad (\text{A.8})$$

$$\partial_t \lambda_1 = \frac{1}{128\pi^2} (3g_1^4 + 9g_2^4 + 6g_1^2(g_2^2 - 4\lambda_1) - 72g_2^2\lambda_1$$

⁸This relates the $\overline{\text{MS}}$ -scale with that of the MS scheme.

$$+ 8(24\lambda_1^2 + 2\lambda_3^2 + 2\lambda_3\lambda_4 + \lambda_4^2 + \lambda_5^2), \quad (\text{A.9})$$

$$\begin{aligned} \partial_t \lambda_2 = & \frac{1}{128\pi^2} \left(3g_1^4 + 9g_2^4 + 6g_1^2(g_2^2 - 4\lambda_2) - 72g_2^2\lambda_2 \right. \\ & \left. + 96\lambda_2(y_t^2 + 2\lambda_2) + 8(-6y_t^4 + 2\lambda_3^2 + 2\lambda_3\lambda_4 + \lambda_4^2 + \lambda_5^2) \right), \end{aligned} \quad (\text{A.10})$$

$$\begin{aligned} \partial_t \lambda_3 = & \frac{1}{64\pi^2} \left(3g_1^4 + 9g_2^4 - 36g_2^2\lambda_3 - 6g_1^2(g_2^2 + 2\lambda_3) \right. \\ & \left. + 8(\lambda_3(3y_t^2 + 6(\lambda_1 + \lambda_2) + 2\lambda_3) + 2(\lambda_1 + \lambda_2)\lambda_4 + \lambda_4^2 + \lambda_5^2) \right), \end{aligned} \quad (\text{A.11})$$

$$\begin{aligned} \partial_t \lambda_4 = & \frac{1}{16\pi^2} \left(3g_1^2(g_2^2 - \lambda_4) + 9g_2^2\lambda_4 + 6y_t^2\lambda_4 \right. \\ & \left. + 4\lambda_4(\lambda_1 + \lambda_2 + 2\lambda_3 + \lambda_4) + 8\lambda_5^2 \right), \end{aligned} \quad (\text{A.12})$$

$$\partial_t \lambda_5 = \frac{1}{16\pi^2} \lambda_5 \left(-3g_1^2 - 9g_2^2 + 6y_t^2 + 4(\lambda_1 + \lambda_2 + 2\lambda_3 + 3\lambda_4) \right), \quad (\text{A.13})$$

The renormalisation scale of the thermal transition is chosen as $\bar{\mu}_4 = 4\pi e^{-\gamma_E} T$, which lies close to the thermal scale and suppresses its contribution to the thermal logarithms. The scales of the soft and ultrasoft EFTs are set to $\bar{\mu}_3 = \bar{\mu}_{3\text{US}} = BT$, and for simplicity we choose $B = 1$. We refer to this choice of the $\bar{\mu}_{3\text{US}}$ scale as the ‘softer’ scale. In practice, the choice of $\bar{\mu}_3$ can be made more rigorous by applying the *principle of minimal sensitivity* [150]. This principle entails minimising the dependence of $\bar{\mu}_3$ or $\bar{\mu}_{3\text{US}}$, for example, in the effective potential, to determine an optimal scale $\bar{\mu}_{\text{opt}}$, as discussed in [151–153].

A.2. Relations between $\overline{\text{MS}}$ -parameters and physical observables

The physical observables map to the $\overline{\text{MS}}$ -parameters of the Lagrangian as,

$$\begin{aligned} (m_h, m_{H^\pm}, m_H, m_A, \cos(\beta - \alpha), \tan(\beta), m_W, m_Z, m_t, G_f, \alpha_s) \\ \Downarrow \\ (m_{11}^2, m_{22}^2, m_{12}^2, \lambda_1, \lambda_2, \lambda_3, \lambda_4, \lambda_5, g_1, g_2, g_3, y_t). \end{aligned} \quad (\text{A.14})$$

The physical observables, along with m_{12} , serve as input parameters measured at the Z -pole, $\mu = m_Z$. We define the shorthand notation $g_0^2 = 4\sqrt{2}G_f m_W^2$ for the tree-level coupling.

At tree level, the vacuum relations for the gauge couplings are,

$$g_1^2 = g_0^2, \quad g_2^2 = g_0^2 \left(\left(\frac{m_Z}{m_W} \right)^2 - 1 \right), \quad g_3^2 = \frac{g_0^2}{2} \left(\frac{m_t}{m_W} \right)^2. \quad (\text{A.15})$$

For the other Lagrangian parameters, we list the tree-level relations given in Appendix B.2

of ref. [46]:

$$m_{11}^2 = m_{12}^2 t_\beta - \frac{1}{2} (m_H^2 + (m_H^2 - m_H^2) c_{\beta-\alpha} (c_{\beta-\alpha} + s_{\beta-\alpha} t_\beta)), \quad (\text{A.16})$$

$$m_{22}^2 = m_{12}^2 t_\beta^{-1} - \frac{1}{2} (m_H^2 + (m_H^2 - m_H^2) c_{\beta-\alpha} (c_{\beta-\alpha} - s_{\beta-\alpha} t_\beta^{-1})), \quad (\text{A.17})$$

$$v^2 \lambda_1 = \frac{1}{2} \left(m_H^2 + \Omega^2 t_\beta^2 - (m_H^2 - m_H^2) (1 - (s_{\beta-\alpha} + c_{\beta-\alpha} t_\beta^{-1})^2) t_\beta^2 \right), \quad (\text{A.18})$$

$$v^2 \lambda_2 = \frac{1}{2} \left(m_H^2 + \Omega^2 t_\beta^{-2} - (m_H^2 - m_H^2) (1 - (s_{\beta-\alpha} - c_{\beta-\alpha} t_\beta)^2) t_\beta^{-2} \right), \quad (\text{A.19})$$

$$v^2 \lambda_3 = 2m_{H^\pm} + \Omega^2 - m_H^2 - (m_H^2 - m_H^2) (1 + (s_{\beta-\alpha} + c_{\beta-\alpha} t_\beta^{-1})(s_{\beta-\alpha} - c_{\beta-\alpha} t_\beta)), \quad (\text{A.20})$$

$$v^2 \lambda_4 = m_A^2 - 2m_H^\pm + m_H^2 - \Omega^2, \quad (\text{A.21})$$

$$v^2 \lambda_5 = m_H^2 - m_A^2 - \Omega^2, \quad (\text{A.22})$$

where we have defined $\Omega^2 \equiv m_H^2 - m_{12}^2 (\tan(\beta) + \tan(\beta)^{-1})$ as in [46],⁹ and we use the notation $c_{\beta-\alpha} = \cos(\beta - \alpha)$ (and likewise for the other trigonometric functions and angles). In appendix A of [47], the one-loop $\overline{\text{MS}}$ renormalised expressions are provided with reference to the self-energies for the gauge bosons, top quark, and the scalars h , H , H^\pm and A . We make use of the self energies calculated by the authors of [47], which have analytic expressions too unwieldy to quote here. Explicit expressions for the self energies can be found in [154]. The one-loop renormalised Lagrangian parameters are also defined at $\mu = m_Z$, like the input physical observables. We then use the beta functions to run them to the thermal scale.

B. Integration of DR EFT into PhaseTracer2

The output of `DRAlgo` can be incredibly long and impractical for computation. With increasing loop orders, the number of binary operations in a single expression for the potential becomes too high for some compilers to parse and optimise. Fortunately, techniques exist to optimise the expressions prior to inserting into code. In Mathematica, after running the dimensional reduction in `DRAlgo`, the `Experimental`OptimizeExpression` function can simplify expressions by identifying common sub-expressions and creating new ‘Compile’ variables to save on evaluation time. The subsequent expression that is composed of Compile variables is subsequently far shorter and can be parsed by compilers.

Additionally, the `CForm` function can allow for the conversion of this optimised expression into C code, with the `StringReplace` function allowing for the manipulation of the subsequent code strings so that they can be adapted for use in Python, C++, or any other programming language. Thus, a function can be created that compounds these operations together such that `DRAlgo` output can readily be used in a programme.

⁹Note that there is a difference in sign between our m_{12}^2 and the one defined in [46].

When interfacing the dimensionally reduced output with `PhaseTracer2`, particular care must be taken so that the package can handle divergences at low temperatures, as this is beyond the validity of the EFT (we remind the reader that the vacuum structure is encoded in the Lagrangian parameters through the vacuum renormalisation of sec. A.2). The `set_t_low` and `set_t_high` functions in the `PhaseFinder` module allows for the temperature bounds to be set, such that phases are only identified between those temperatures and numerical issues can be avoided.

Finally, regarding the parameter scans: `PhaseTracer2` does not come with an interface to set them up. However, it is relatively straightforward to wrap the `PhaseTracer2` objects in a class that can be instantiated with the a new set of parameters. Parallelisation of the scan across multiple threads allows for increased efficiency when computing results, particularly on machines with numerous cores.

References

- [1] **ATLAS** Collaboration, G. Aad *et al.*, *Observation of a new particle in the search for the Standard Model Higgs boson with the ATLAS detector at the LHC*, Phys. Lett. B **716** (2012) 1 [1207.7214].
- [2] **CMS** Collaboration, S. Chatrchyan *et al.*, *Observation of a New Boson at a Mass of 125 GeV with the CMS Experiment at the LHC*, Phys. Lett. B **716** (2012) 30 [1207.7235].
- [3] **CMS** Collaboration, A. M. Sirunyan *et al.*, *Search for a standard model-like Higgs boson in the mass range between 70 and 110 GeV in the diphoton final state in proton-proton collisions at $\sqrt{s} = 8$ and 13 TeV*, Phys. Lett. B **793** (2019) 320 [1811.08459].
- [4] **CMS** Collaboration, A. Hayrapetyan *et al.*, *Search for a standard model-like Higgs boson in the mass range between 70 and 110 GeV in the diphoton final state in proton-proton collisions at $s=13$ TeV*, Phys. Lett. B **860** (2025) 139067 [2405.18149].
- [5] **ATLAS** Collaboration, *Search for diphoton resonances in the 66 to 110 GeV mass range using 140 fb^{-1} of 13 TeV pp collisions collected with the ATLAS detector*, tech. rep., CERN, Geneva, 2023.
- [6] **CMS** Collaboration, A. Tumasyan *et al.*, *Searches for additional Higgs bosons and for vector leptoquarks in $\tau\tau$ final states in proton-proton collisions at $\sqrt{s} = 13$ TeV*, JHEP **07** (2023) 073 [2208.02717].
- [7] **ALEPH, DELPHI, L3, OPAL, LEP Working Group for Higgs Boson Searches** Collaboration, S. Schael *et al.*, *Search for neutral MSSM Higgs bosons at LEP*, Eur. Phys. J. C **47** (2006) 547 [hep-ex/0602042].
- [8] A. Belyaev, R. Benbrik, M. Boukidi, M. Chakraborti, S. Moretti, and S. Semmlali, *Explanation of the hints for a 95 GeV Higgs boson within a 2-Higgs Doublet Model*, JHEP **05** (2024) 209 [2306.09029].

- [9] J. Cao, X. Guo, Y. He, P. Wu, and Y. Zhang, *Diphoton signal of the light Higgs boson in natural NMSSM*, Phys. Rev. D **95** (2017) 116001 [1612.08522].
- [10] S. Heinemeyer, C. Li, F. Lika, G. Moortgat-Pick, and S. Paasch, *Phenomenology of a 96 GeV Higgs boson in the 2HDM with an additional singlet*, Phys. Rev. D **106** (2022) 075003 [2112.11958].
- [11] T. Biekötter, M. Chakraborti, and S. Heinemeyer, *A 96 GeV Higgs boson in the N2HDM*, Eur. Phys. J. C **80** (2020) 2 [1903.11661].
- [12] T. Biekötter and M. O. Olea-Romacho, *Reconciling Higgs physics and pseudo-Nambu-Goldstone dark matter in the S2HDM using a genetic algorithm*, JHEP **10** (2021) 215 [2108.10864].
- [13] T. Biekötter, A. Grohsjean, S. Heinemeyer, C. Schwanenberger, and G. Weiglein, *Possible indications for new Higgs bosons in the reach of the LHC: N2HDM and NMSSM interpretations*, Eur. Phys. J. C **82** (2022) 178 [2109.01128].
- [14] T. Biekötter, S. Heinemeyer, and G. Weiglein, *Mounting evidence for a 95 GeV Higgs boson*, JHEP **08** (2022) 201 [2203.13180].
- [15] T. Biekötter, S. Heinemeyer, and G. Weiglein, *Excesses in the low-mass Higgs-boson search and the W-boson mass measurement*, Eur. Phys. J. C **83** (2023) 450 [2204.05975].
- [16] T. Biekötter, S. Heinemeyer, and G. Weiglein, *The CMS di-photon excess at 95 GeV in view of the LHC Run 2 results*, Phys. Lett. B **846** (2023) 138217 [2303.12018].
- [17] T. Biekötter, S. Heinemeyer, and G. Weiglein, *95.4 GeV diphoton excess at ATLAS and CMS*, Phys. Rev. D **109** (2024) 035005 [2306.03889].
- [18] J. Cao, X. Jia, Y. Yue, H. Zhou, and P. Zhu, *96 GeV diphoton excess in seesaw extensions of the natural NMSSM*, Phys. Rev. D **101** (2020) 055008 [1908.07206].
- [19] S. Iguro, T. Kitahara, and Y. Omura, *Scrutinizing the 95–100 GeV di-tau excess in the top associated process*, Eur. Phys. J. C **82** (2022) 1053 [2205.03187].
- [20] W. Li, H. Qiao, and J. Zhu, *Light Higgs boson in the NMSSM confronted with the CMS di-photon and di-tau excesses**, Chin. Phys. C **47** (2023) 123102 [2212.11739].
- [21] J. M. Cline and T. Toma, *Pseudo-Goldstone dark matter confronts cosmic ray and collider anomalies*, Phys. Rev. D **100** (2019) 035023 [1906.02175].
- [22] A. Crivellin, J. Heck, and D. Müller, *Large $h \rightarrow bs$ in generic two-Higgs-doublet models*, Phys. Rev. D **97** (2018) 035008 [1710.04663].
- [23] G. Cacciapaglia, A. Deandrea, S. Gascon-Shotkin, S. Le Corre, M. Lethuillier, and J. Tao, *Search for a lighter Higgs boson in Two Higgs Doublet Models*, JHEP **12** (2016) 068 [1607.08653].
- [24] A. A. Abdelalim, B. Das, S. Khalil, and S. Moretti, *Di-photon decay of a light Higgs state in the BLSSM*, Nucl. Phys. B **985** (2022) 116013 [2012.04952].
- [25] D. Azevedo, T. Biekötter, and P. M. Ferreira, *2HDM interpretations of the CMS diphoton excess at 95 GeV*, JHEP **11** (2023) 017 [2305.19716].

- [26] R. Benbrik, M. Boukidi, and S. Moretti, *Superposition of CP-even and CP-odd Higgs resonances: Explaining the 95 GeV excesses within a two-Higgs-doublet model*, Phys. Rev. D **110** (2024) 115030 [2405.02899].
- [27] A. Arhrib, K. H. Phan, V. Q. Tran, and T.-C. Yuan, *When the Standard Model Higgs meets its lighter 95 GeV twin*, Nucl. Phys. B **1015** (2025) 116909.
- [28] J. A. Aguilar-Saavedra, H. B. Câmara, F. R. Joaquim, and J. F. Seabra, *Confronting the 95 GeV excesses within the $U(1)$ '-extended next-to-minimal 2HDM*, Phys. Rev. D **108** (2023) 075020 [2307.03768].
- [29] A. Belyaev, R. Benbrik, M. Boukidi, M. Chakraborti, S. Moretti, and S. Semlali, *Probing 95 GeV Higgs in the 2HDM Type-III*, PoS LHCP2023 (2024) 299 [2402.03998].
- [30] K. Kajantie, M. Laine, K. Rummukainen, and M. E. Shaposhnikov, *Generic rules for high temperature dimensional reduction and their application to the standard model*, Nucl. Phys. B **458** (1996) 90 [hep-ph/9508379].
- [31] E. Braaten and A. Nieto, *Effective field theory approach to high temperature thermodynamics*, Phys. Rev. D **51** (1995) 6990 [hep-ph/9501375].
- [32] J. M. Cline, K. Kainulainen, and A. P. Vischer, *Dynamics of two Higgs doublet CP violation and baryogenesis at the electroweak phase transition*, Phys. Rev. D **54** (1996) 2451 [hep-ph/9506284].
- [33] L. Fromme, S. J. Huber, and M. Seniuch, *Baryogenesis in the two-Higgs doublet model*, JHEP **11** (2006) 038 [hep-ph/0605242].
- [34] I. P. Ivanov, *Thermal evolution of the ground state of the most general 2HDM*, Acta Phys. Polon. B **40** (2009) 2789 [0812.4984].
- [35] I. F. Ginzburg, I. P. Ivanov, and K. A. Kanishev, *The Evolution of vacuum states and phase transitions in 2HDM during cooling of Universe*, Phys. Rev. D **81** (2010) 085031 [0911.2383].
- [36] G. C. Dorsch, S. J. Huber, and J. M. No, *A strong electroweak phase transition in the 2HDM after LHC8*, JHEP **10** (2013) 029 [1305.6610].
- [37] P. Basler, M. Krause, M. Muhlleitner, J. Wittbrodt, and A. Wlotzka, *Strong First Order Electroweak Phase Transition in the CP-Conserving 2HDM Revisited*, JHEP **02** (2017) 121 [1612.04086].
- [38] G. C. Dorsch, S. J. Huber, T. Konstandin, and J. M. No, *A Second Higgs Doublet in the Early Universe: Baryogenesis and Gravitational Waves*, JCAP **05** (2017) 052 [1611.05874].
- [39] W. Grimus, L. Lavoura, O. M. Ogreid, and P. Osland, *A Precision constraint on multi-Higgs-doublet models*, J. Phys. G **35** (2008) 075001 [0711.4022].
- [40] H. E. Haber and D. O'Neil, *Basis-independent methods for the two-Higgs-doublet model III: The CP-conserving limit, custodial symmetry, and the oblique parameters S , T , U* , Phys. Rev. D **83** (2011) 055017 [1011.6188].
- [41] G. Funk, D. O'Neil, and R. M. Winters, *What the Oblique Parameters S , T , and U and Their Extensions Reveal About the 2HDM: A Numerical Analysis*, Int. J. Mod. Phys. A **27** (2012) 1250021 [1110.3812].

- [42] H. E. Haber and H. E. Logan, *Radiative corrections to the $Z b$ anti- b vertex and constraints on extended Higgs sectors*, Phys. Rev. D **62** (2000) 015011 [hep-ph/9909335].
- [43] M. Jung, A. Pich, and P. Tuzon, *Charged-Higgs phenomenology in the Aligned two-Higgs-doublet model*, JHEP **11** (2010) 003 [1006.0470].
- [44] J. O. Andersen, T. Gorda, A. Helset, *et al.*, *Nonperturbative Analysis of the Electroweak Phase Transition in the Two Higgs Doublet Model*, Phys. Rev. Lett. **121** (2018) 191802 [1711.09849].
- [45] A. Helset, *Dimensional reduction of the Two-Higgs Doublet Model with a softly broken Z_2 symmetry at one-loop*, Master's thesis, Norwegian U. Sci. Tech., 6, 2017.
- [46] T. Gorda, A. Helset, L. Niemi, T. V. I. Tenkanen, and D. J. Weir, *Three-dimensional effective theories for the two Higgs doublet model at high temperature*, JHEP **02** (2019) 081 [1802.05056].
- [47] K. Kainulainen, V. Keus, L. Niemi, K. Rummukainen, T. V. I. Tenkanen, and V. Vaskonen, *On the validity of perturbative studies of the electroweak phase transition in the Two Higgs Doublet model*, JHEP **06** (2019) 075 [1904.01329].
- [48] M. Losada, *High temperature dimensional reduction of the MSSM and other multiscalar models*, Phys. Rev. D **56** (1997) 2893 [hep-ph/9605266].
- [49] J. O. Andersen, *Dimensional reduction of the two Higgs doublet model at high temperature*, Eur. Phys. J. C **11** (1999) 563 [hep-ph/9804280].
- [50] M. Laine and K. Rummukainen, *Two Higgs doublet dynamics at the electroweak phase transition: A Nonperturbative study*, Nucl. Phys. B **597** (2001) 23 [hep-lat/0009025].
- [51] M. Laine, M. Meyer, and G. Nardini, *Thermal phase transition with full 2-loop effective potential*, Nucl. Phys. B **920** (2017) 565 [1702.07479].
- [52] I. K. Banerjee, U. K. Dey, and S. Khalil, *Primordial Black Holes and Gravitational Waves in the $U(1)_{B-L}$ extended inert doublet model: a first-order phase transition perspective*, JHEP **12** (2024) 009 [2406.12518].
- [53] S. Jiang, F. P. Huang, and X. Wang, *Bubble wall velocity during electroweak phase transition in the inert doublet model*, Phys. Rev. D **107** (2023) 095005 [2211.13142].
- [54] K. Kajantie, M. Laine, K. Rummukainen, and M. E. Shaposhnikov, *Is there a hot electroweak phase transition at $m_H \gtrsim m_W$?*, Phys. Rev. Lett. **77** (1996) 2887 [hep-ph/9605288].
- [55] K. Kajantie, M. Laine, K. Rummukainen, and M. E. Shaposhnikov, *A Nonperturbative analysis of the finite T phase transition in $SU(2) \times U(1)$ electroweak theory*, Nucl. Phys. B **493** (1997) 413 [hep-lat/9612006].
- [56] M. Gurtler, E.-M. Ilgenfritz, and A. Schiller, *Where the electroweak phase transition ends*, Phys. Rev. D **56** (1997) 3888 [hep-lat/9704013].
- [57] F. Csikor, Z. Fodor, and J. Heitger, *Endpoint of the hot electroweak phase transition*, Phys. Rev. Lett. **82** (1999) 21 [hep-ph/9809291].
- [58] M. D'Onofrio and K. Rummukainen, *Standard model cross-over on the lattice*, Phys. Rev. D **93** (2016) 025003 [1508.07161].

- [59] L. Niemi, M. J. Ramsey-Musolf, T. V. I. Tenkanen, and D. J. Weir, *Thermodynamics of a Two-Step Electroweak Phase Transition*, Phys. Rev. Lett. **126** (2021) 171802 [2005.11332].
- [60] C. Caprini *et al.*, *Science with the space-based interferometer eLISA. II: Gravitational waves from cosmological phase transitions*, JCAP **04** (2016) 001 [1512.06239].
- [61] C. Caprini *et al.*, *Detecting gravitational waves from cosmological phase transitions with LISA: an update*, JCAP **03** (2020) 024 [1910.13125].
- [62] **LISA Cosmology Working Group** Collaboration, P. Auclair *et al.*, *Cosmology with the Laser Interferometer Space Antenna*, Living Rev. Rel. **26** (2023) 5 [2204.05434].
- [63] G. M. Harry, P. Fritschel, D. A. Shaddock, W. Folkner, and E. S. Phinney, *Laser interferometry for the big bang observer*, Class. Quant. Grav. **23** (2006) 4887.
- [64] S. Kawamura *et al.*, *The Japanese space gravitational wave antenna: DECIGO*, Class. Quant. Grav. **28** (2011) 094011.
- [65] W.-H. Ruan, Z.-K. Guo, R.-G. Cai, and Y.-Z. Zhang, *Taiji program: Gravitational-wave sources*, Int. J. Mod. Phys. A **35** (2020) 2050075 [1807.09495].
- [66] M. J. Ramsey-Musolf, V. Q. Tran, and T.-C. Yuan, *Gravitational waves and dark matter in the gauged two-Higgs doublet model*, JHEP **01** (2025) 129 [2408.05167].
- [67] S. Lee, D. Kim, J.-H. Cho, J. Kim, and J. Song, *Multi-step Strong First-Order Electroweak Phase Transitions in the Inverted Type-I 2HDM: Parameter Space, Gravitational Waves, and Collider Phenomenology*, [2506.03260].
- [68] D. Gonçalves, A. Kaladharan, and Y. Wu, *Gravitational waves, bubble profile, and baryon asymmetry in the complex 2HDM*, Phys. Rev. D **108** (2023) 075010 [2307.03224].
- [69] R. Zhou and L. Bian, *Gravitational wave and electroweak baryogenesis with two Higgs doublet models*, Phys. Lett. B **829** (2022) 137105 [2001.01237].
- [70] T. Biekötter, S. Heinemeyer, J. M. No, M. O. Olea-Romacho, and G. Weiglein, *The trap in the early Universe: impact on the interplay between gravitational waves and LHC physics in the 2HDM*, JCAP **03** (2023) 031 [2208.14466].
- [71] P. J. Fox and N. Weiner, *Light Signals from a Lighter Higgs*, JHEP **08** (2018) 025 [1710.07649].
- [72] G. C. Branco, P. M. Ferreira, L. Lavoura, M. N. Rebelo, M. Sher, and J. P. Silva, *Theory and phenomenology of two-Higgs-doublet models*, Phys. Rept. **516** (2012) 1 [1106.0034].
- [73] A. Bernal, J. A. Casas, and J. M. Moreno, *Fine-tuning in the 2HDM*, Eur. Phys. J. C **82** (2022) 950 [2202.09103].
- [74] S. L. Glashow and S. Weinberg, *Natural Conservation Laws for Neutral Currents*, Phys. Rev. D **15** (1977) 1958.
- [75] E. A. Paschos, *Diagonal Neutral Currents*, Phys. Rev. D **15** (1977) 1966.
- [76] J. Bernon, J. F. Gunion, H. E. Haber, Y. Jiang, and S. Kraml, *Scrutinizing the alignment limit in two-Higgs-doublet models: $m_h=125$ GeV*, Phys. Rev. D **92** (2015) 075004 [1507.00933].

- [77] P. H. Ginsparg, *First Order and Second Order Phase Transitions in Gauge Theories at Finite Temperature*, Nucl. Phys. B **170** (1980) 388.
- [78] T. Appelquist and R. D. Pisarski, *High-Temperature Yang-Mills Theories and Three-Dimensional Quantum Chromodynamics*, Phys. Rev. D **23** (1981) 2305.
- [79] S. Nadkarni, *Dimensional Reduction in Hot QCD*, Phys. Rev. D **27** (1983) 917.
- [80] N. P. Landsman, *Limitations to Dimensional Reduction at High Temperature*, Nucl. Phys. B **322** (1989) 498.
- [81] E. Braaten and A. Nieto, *Free energy of QCD at high temperature*, Phys. Rev. D **53** (1996) 3421 [hep-ph/9510408].
- [82] D. Croon, O. Gould, P. Schicho, T. V. I. Tenkanen, and G. White, *Theoretical uncertainties for cosmological first-order phase transitions*, JHEP **04** (2021) 055 [2009.10080].
- [83] O. Gould and T. V. I. Tenkanen, *On the perturbative expansion at high temperature and implications for cosmological phase transitions*, JHEP **06** (2021) 069 [2104.04399].
- [84] M. Lewicki, M. Merchand, L. Sagunski, P. Schicho, and D. Schmitt, *Impact of theoretical uncertainties on model parameter reconstruction from GW signals sourced by cosmological phase transitions*, Phys. Rev. D **110** (2024) 023538 [2403.03769].
- [85] C. Grojean and G. Servant, *Gravitational Waves from Phase Transitions at the Electroweak Scale and Beyond*, Phys. Rev. D **75** (2007) 043507 [hep-ph/0607107].
- [86] C. Delaunay, C. Grojean, and J. D. Wells, *Dynamics of Non-renormalizable Electroweak Symmetry Breaking*, JHEP **04** (2008) 029 [0711.2511].
- [87] J. Ellis, M. Lewicki, and J. M. No, *On the Maximal Strength of a First-Order Electroweak Phase Transition and its Gravitational Wave Signal*, JCAP **04** (2019) 003 [1809.08242].
- [88] T. Matsubara, *A New approach to quantum statistical mechanics*, Prog. Theor. Phys. **14** (1955) 351.
- [89] A. D. Linde, *Infrared Problem in Thermodynamics of the Yang-Mills Gas*, Phys. Lett. B **96** (1980) 289.
- [90] J. Hirvonen, *Intuitive method for constructing effective field theories*, [2205.02687].
- [91] O. Gould and J. Hirvonen, *Effective field theory approach to thermal bubble nucleation*, Phys. Rev. D **104** (2021) 096015 [2108.04377].
- [92] O. Gould and T. V. I. Tenkanen, *Perturbative effective field theory expansions for cosmological phase transitions*, JHEP **01** (2024) 048 [2309.01672].
- [93] A. Ekstedt, P. Schicho, and T. V. I. Tenkanen, *DRalgo: A package for effective field theory approach for thermal phase transitions*, Comput. Phys. Commun. **288** (2023) 108725 [2205.08815].
- [94] B. Ruijl, T. Ueda, and J. Vermaseren, *FORM version 4.2* [1707.06453].
- [95] P. Nogueira, *Automatic Feynman Graph Generation*, J. Comput. Phys. **105** (1993) 279.

- [96] A. Ekstedt, O. Gould, and J. Löfgren, *Radiative first-order phase transitions to next-to-next-to-leading order*, Phys. Rev. D **106** (2022) 036012 [2205.07241].
- [97] A. Ekstedt, P. Schicho, and T. V. I. Tenkanen, *Cosmological phase transitions at three loops: The final verdict on perturbation theory*, Phys. Rev. D **110** (2024) 096006 [2405.18349].
- [98] P. Schicho, T. V. I. Tenkanen, and G. White, *Combining thermal resummation and gauge invariance for electroweak phase transition*, JHEP **11** (2022) 047 [2203.04284].
- [99] S. R. Coleman and E. J. Weinberg, *Radiative Corrections as the Origin of Spontaneous Symmetry Breaking*, Phys. Rev. D **7** (1973) 1888.
- [100] L. Niemi, P. Schicho, and T. V. I. Tenkanen, *Singlet-assisted electroweak phase transition at two loops*, Phys. Rev. D **103** (2021) 115035 [2103.07467].
- [101] P. Athron, C. Balázs, A. Fowlie, and Y. Zhang, *PhaseTracer: tracing cosmological phases and calculating transition properties*, Eur. Phys. J. C **80** (2020) 567 [2003.02859].
- [102] P. Athron, C. Balazs, A. Fowlie, *et al.*, *PhaseTracer2: from the effective potential to gravitational waves*, Eur. Phys. J. C **85** (2025) 559 [2412.04881].
- [103] **LISA Study Team** Collaboration, K. Danzmann, *LISA mission overview*, Adv. Space Res. **25** (2000) 1129.
- [104] S. R. Coleman, *The Fate of the False Vacuum. 1. Semiclassical Theory*, Phys. Rev. D **15** (1977) 2929.
- [105] A. Andreassen, D. Farhi, W. Frost, and M. D. Schwartz, *Precision decay rate calculations in quantum field theory*, Phys. Rev. D **95** (2017) 085011 [1604.06090].
- [106] D. Croon, *TASI lectures on Phase Transitions, Baryogenesis, and Gravitational Waves*, PoS **TASI2022** (2024) 003 [2307.00068].
- [107] A. H. Guth and S. H. H. Tye, *Phase Transitions and Magnetic Monopole Production in the Very Early Universe*, Phys. Rev. Lett. **44** (1980) 631.
- [108] A. H. Guth and E. J. Weinberg, *Cosmological Consequences of a First Order Phase Transition in the SU(5) Grand Unified Model*, Phys. Rev. D **23** (1981) 876.
- [109] M. B. Hindmarsh, M. Lüben, J. Lumma, and M. Pauly, *Phase transitions in the early universe*, SciPost Phys. Lect. Notes **24** (2021) 1 [2008.09136].
- [110] K. Enqvist, J. Ignatius, K. Kajantie, and K. Rummukainen, *Nucleation and bubble growth in a first order cosmological electroweak phase transition*, Phys. Rev. D **45** (1992) 3415.
- [111] M. E. Carrington and J. I. Kapusta, *Dynamics of the electroweak phase transition*, Phys. Rev. D **47** (1993) 5304.
- [112] A. Ekstedt, *Higher-order corrections to the bubble-nucleation rate at finite temperature*, Eur. Phys. J. C **82** (2022) 173 [2104.11804].
- [113] A. Ekstedt, O. Gould, and J. Hirvonen, *BubbleDet: a Python package to compute functional determinants for bubble nucleation*, JHEP **12** (2023) 056 [2308.15652].

- [114] X. Wang, C. Tian, and C. Balázs, *Self-consistent prediction of gravitational waves from cosmological phase transitions*, [2409.06599].
- [115] C. Tian, X. Wang, and C. Balázs, *Gravitational waves from cosmological first-order phase transitions with precise hydrodynamics*, [2409.14505].
- [116] W.-Y. Ai, B. Laurent, and J. van de Vis, *Model-independent bubble wall velocities in local thermal equilibrium*, JCAP **07** (2023) 002 [2303.10171].
- [117] B. Laurent and J. M. Cline, *First principles determination of bubble wall velocity*, Phys. Rev. D **106** (2022) 023501 [2204.13120].
- [118] A. Ekstedt, O. Gould, J. Hirvonen, *et al.*, *How fast does the WallGo? A package for computing wall velocities in first-order phase transitions*, JHEP **04** (2025) 101 [2411.04970].
- [119] P. J. Steinhardt, *Relativistic Detonation Waves and Bubble Growth in False Vacuum Decay*, Phys. Rev. D **25** (1982) 2074.
- [120] M. Laine, *Bubble growth as a detonation*, Phys. Rev. D **49** (1994) 3847 [hep-ph/9309242].
- [121] W.-Y. Ai, B. Garbrecht, and C. Tamarit, *Bubble wall velocities in local equilibrium*, JCAP **03** (2022) 015 [2109.13710].
- [122] W.-Y. Ai, B. Laurent, and J. van de Vis, *Bounds on the bubble wall velocity*, JHEP **02** (2025) 119 [2411.13641].
- [123] T. Krajewski, M. Lewicki, and M. Zych, *Bubble-wall velocity in local thermal equilibrium: hydrodynamical simulations vs analytical treatment*, JHEP **05** (2024) 011 [2402.15408].
- [124] F. Giese, T. Konstandin, and J. van de Vis, *Model-independent energy budget of cosmological first-order phase transitions—A sound argument to go beyond the bag model*, JCAP **07** (2020) 057 [2004.06995].
- [125] T. V. I. Tenkanen and J. van de Vis, *Speed of sound in cosmological phase transitions and effect on gravitational waves*, JHEP **08** (2022) 302 [2206.01130].
- [126] E. Witten, *Cosmic Separation of Phases*, Phys. Rev. D **30** (1984) 272.
- [127] C. J. Hogan, *Gravitational radiation from cosmological phase transitions*, Mon. Not. Roy. Astron. Soc. **218** (1986) 629.
- [128] J. R. Espinosa, T. Konstandin, J. M. No, and G. Servant, *Energy Budget of Cosmological First-order Phase Transitions*, JCAP **06** (2010) 028 [1004.4187].
- [129] F. Giese, T. Konstandin, K. Schmitz, and J. van de Vis, *Model-independent energy budget for LISA*, JCAP **01** (2021) 072 [2010.09744].
- [130] A. Kosowsky and M. S. Turner, *Gravitational radiation from colliding vacuum bubbles: envelope approximation to many bubble collisions*, Phys. Rev. D **47** (1993) 4372 [astro-ph/9211004].
- [131] C. Caprini, R. Durrer, and G. Servant, *The stochastic gravitational wave background from turbulence and magnetic fields generated by a first-order phase transition*, JCAP **12** (2009) 024 [0909.0622].

- [132] A. Roper Pol, S. Mandal, A. Brandenburg, T. Kahniashvili, and A. Kosowsky, *Numerical simulations of gravitational waves from early-universe turbulence*, Phys. Rev. D **102** (2020) 083512 [1903.08585].
- [133] M. Hindmarsh, S. J. Huber, K. Rummukainen, and D. J. Weir, *Gravitational waves from the sound of a first order phase transition*, Phys. Rev. Lett. **112** (2014) 041301 [1304.2433].
- [134] M. Hindmarsh, S. J. Huber, K. Rummukainen, and D. J. Weir, *Numerical simulations of acoustically generated gravitational waves at a first order phase transition*, Phys. Rev. D **92** (2015) 123009 [1504.03291].
- [135] J. Ellis, M. Lewicki, J. M. No, and V. Vaskonen, *Gravitational wave energy budget in strongly supercooled phase transitions*, JCAP **06** (2019) 024 [1903.09642].
- [136] M. Hindmarsh, S. J. Huber, K. Rummukainen, and D. J. Weir, *Shape of the acoustic gravitational wave power spectrum from a first order phase transition*, Phys. Rev. D **96** (2017) 103520 [1704.05871].
- [137] T. L. Smith, T. L. Smith, R. R. Caldwell, and R. Caldwell, *LISA for Cosmologists: Calculating the Signal-to-Noise Ratio for Stochastic and Deterministic Sources*, Phys. Rev. D **100** (2019) 104055 [1908.00546].
- [138] T. J. Sumner, G. Mueller, J. W. Conklin, P. J. Wass, and D. Hollington, *Charge Induced Acceleration Noise in the LISA Gravitational Reference Sensor*, Class. Quant. Grav. **37** (2020) 045010 [1909.12608].
- [139] D. H. Lyth and A. Riotto, *Particle physics models of inflation and the cosmological density perturbation*, Phys. Rept. **314** (1999) 1 [hep-ph/9807278].
- [140] L. Sagunski, P. Schicho, and D. Schmitt, *Supercool exit: Gravitational waves from QCD-triggered conformal symmetry breaking*, Phys. Rev. D **107** (2023) 123512 [2303.02450].
- [141] M. Kierkla, A. Karam, and B. Swiezewska, *Conformal model for gravitational waves and dark matter: a status update*, JHEP **03** (2023) 007 [2210.07075].
- [142] M. Kierkla, B. Swiezewska, T. V. I. Tenkanen, and J. van de Vis, *Gravitational waves from supercooled phase transitions: dimensional transmutation meets dimensional reduction*, JHEP **02** (2024) 234 [2312.12413].
- [143] M. Kierkla, P. Schicho, B. Swiezewska, T. V. I. Tenkanen, and J. van de Vis, *Finite-temperature bubble nucleation with shifting scale hierarchies*, [2503.13597].
- [144] O. Gould and C. Xie, *Higher orders for cosmological phase transitions: a global study in a Yukawa model*, JHEP **12** (2023) 049 [2310.02308].
- [145] M. Chala, J. C. Criado, L. Gil, and J. L. Miras, *Higher-order-operator corrections to phase-transition parameters in dimensional reduction*, JHEP **10** (2024) 025 [2406.02667].
- [146] M. Chala and G. Guedes, *The High-Temperature Limit of the SM(EFT)*, [2503.20016].
- [147] F. Bernardo, P. Klose, P. Schicho, and T. V. I. Tenkanen, *Higher-dimensional operators at finite-temperature affect gravitational-wave predictions*, [2503.18904].

- [148] L. S. Friedrich, M. J. Ramsey-Musolf, T. V. I. Tenkanen, and V. Q. Tran, *Addressing the Gravitational Wave - Collider Inverse Problem*, [2203.05889].
- [149] M. J. Ramsey-Musolf, T. V. I. Tenkanen, and V. Q. Tran, *Refining Gravitational Wave and Collider Physics Dialogue via Singlet Scalar Extension*, [2409.17554].
- [150] P. M. Stevenson, *Optimized Perturbation Theory*, Phys. Rev. D **23** (1981) 2916.
- [151] S.-z. Huang and M. Lissia, *The Relevant scale parameter in the high temperature phase of QCD*, Nucl. Phys. B **438** (1995) 54 [hep-ph/9411293].
- [152] M. Laine and Y. Schroder, *Two-loop QCD gauge coupling at high temperatures*, JHEP **03** (2005) 067 [hep-ph/0503061].
- [153] I. Ghisoiu, J. Moller, and Y. Schroder, *Debye screening mass of hot Yang-Mills theory to three-loop order*, JHEP **11** (2015) 121 [1509.08727].
- [154] S. Kanemura, M. Kikuchi, and K. Yagyu, *Fingerprinting the extended Higgs sector using one-loop corrected Higgs boson couplings and future precision measurements*, Nucl. Phys. B **896** (2015) 80 [1502.07716].